

Magnetic evidence for hot superconductivity in multi-walled carbon nanotubes

Guo-meng Zhao* and Pieder Beeli

Department of Physics and Astronomy, California State University, Los Angeles, CA 90032, USA

We report magnetic measurements up to 1200 K on three different multi-walled carbon nanotube mat samples using Quantum Design vibrating sample magnetometers. Three different samples prepared from arc discharge or chemical vapor deposition contain magnetic impurities ranging from about 100 ppm to about 1.5%. Our precise magnetic data clearly show two superconducting transitions, one at temperatures between 533 K and 700 K, and another at about 1200 K. The first transition temperature T_{cJ} , which coincides with the transition temperature seen in the resistance data, depends very strongly on the magnetic field, as expected from the onset of intergrain Josephson coupling in granular superconductors. The strong field dependence of T_{cJ} also excludes magnetic contaminants as the origin of the first transition. We also present direct and inferred diamagnetic Meissner fractions of 2 and 14%, respectively. The present results provide compelling evidence for superconductivity well above room temperature in multi-walled carbon nanotubes.

I. INTRODUCTION

It is generally believed that the superconducting transition temperature T_c cannot be higher than 30 K within the conventional phonon-mediated mechanism. Alexandrov and Mott have demonstrated that the Bose-Einstein condensation of bipolarons can explain high-temperature superconductivity in cuprates [1]. Ginzburg [2] and Little [3] have proposed that high-temperature superconductivity could be realized by exchanging high-energy electronic excitations such as excitons and plasmons. Lee and Mendoza have shown that superconductivity as high as 500 K can be reached through a pairing interaction mediated by undamped acoustic plasmon modes in a quasi-one-dimensional (1D) electronic system [4]. Moreover, high-temperature superconductivity can occur in a multi-layer electronic system due to an attraction of charge carriers in the same conducting layer via exchange of virtual plasmons in neighboring layers [5]. If these plasmon-mediated pairing mechanisms are relevant, one should be able to find high-temperature superconductivity in quasi-one-dimensional and/or multi-layer systems such as cuprates, carbon nanotubes (CNTs), and graphites.

Carbon nanotubes constitute a novel class of quasi-one-dimensional materials which offer the potential for high-temperature superconductivity. The simplest single-walled nanotube (SWNT) consists of a single graphite sheet which is curved into a long cylinder, with a diameter which can be smaller than 1 nm. Band-structure calculations predict that carbon nanotubes have two types of electronic structures depending on the chirality [6,7], which is indexed by a chiral vector (n, m) : $n - m = 3I + \nu$, where I, n, m are the integers, and $\nu = 0, \pm 1$. The tubes with $\nu = 0$ are metallic while the tubes with $\nu = \pm 1$ are semiconducting. For metallic chirality SWNTs, there are two and six transverse conduction channels when the Fermi level is crossing the first and second subbands, respectively. Multiwalled nanotubes (MWNTs) consist of at least two concentric shells which

can have different chiralities. The outer diameters of our arc discharge prepared MWNTs are centered at around 10-15 nm. MWNTs possess both quasi-one-dimensional and multi-layer electronic structures. This unique quasi-one-dimensional electronic structure in both SWNTs and MWNTs make them ideal for plasmon-mediated high-temperature superconductivity.

In order to confirm the existence of superconductivity, it is essential to provide two important signatures: the Meissner effect and the resistive transition. In 2001 Zhao *et al.* [8] provided magnetic and electrical evidence for possible superconductivity above room temperature in MWNT mat samples. The resistivity data show a possible superconductive transition at about 700 K. Since then, Zhao [9,10] has analyzed previously published magnetic, electrical, and optical data for both single-walled and multi-walled carbon nanotubes, and provided over twenty arguments for the existence of hot superconductivity. In 2003, Kopelevich and coworkers [11] gave magnetic evidence for local superconductivity up to 270 K in graphite-sulfur composites. The observations of hot superconductivity in carbon nanotubes and graphite-sulfur composites suggest a common microscopic origin of superconductivity.

In this article, we report magnetic measurements up to 1200 K on three different multi-walled carbon nanotube mat samples using sensitive vibrating sample magnetometers (VSMs) from Quantum Design. The ultra low-field option of the VSM system allows us to do the magnetization measurements in a field as low as 0.03 Oe. One sample is prepared from arc discharge (denoted as AD) and contains about 100 ppm magnetic impurities. The second sample is prepared from chemical vapor deposition (denoted as CVD1) and contains about 1.5% Fe_3O_4 . The third sample is also prepared from chemical vapor deposition (denoted as CVD2) and has about 0.3% impurities. Our extensive magnetic data consistently show two superconducting transitions, one at about 700 K, 533 K, and 700 K for sample AD, sample CVD1 and

sample CVD2, respectively, and another at about 1200 K. The first transition temperature T_{cJ} , which coincides with the transition temperature seen in the previous resistance data [8], depends very strongly on the magnetic field in the low field range, as expected from the onset of intergrain Josephson coupling in granular superconductors. The strong field dependence of T_{cJ} also excludes magnetic contaminants as the origin of the first transition. We also present direct and inferred diamagnetic Meissner fractions of 2 and 14%, respectively. Such a large field-cooled diamagnetic susceptibility is *only* consistent with superconductivity. The superconducting remanent magnetization, which can be distinguished from the remanent contribution of magnetic impurities, exists up to 700 K, indicating a zero-resistance state well above room-temperature in some parts of the mat samples. The present results provide compelling evidence for superconductivity well above room temperature in multi-walled carbon nanotubes.

II. EXPERIMENT

A. Sample characterization

Three different multi-walled carbon nanotube mat samples are obtained from SES Research of Houston. Sample AD is prepared from an arc discharge process with no metal catalysts. The multi-walled nanotubes consist of 5-20 graphite layers with diameters between 2 and 20 nm and lengths between 100 nm and 2 μm . The tubes are naturally assembled into bundles, and the bundles into mats where bundles are entangled with each other. Sample AD comes from the same lot as those studied in Ref. [8]. This sample contains a total of about 100 ppm magnetic impurities, as determined from the magnetic measurement (see below). The mass of sample AD is 41 mg for most magnetic measurements. Sample CVD1 is prepared from chemical vapor deposition and contains about 1.5% Fe_3O_4 . The mass of sample CVD1 is 5 mg. Sample CVD2 is also prepared from chemical vapor deposition and contains a total of about 0.3% impurities. The mass of sample CVD2 is 11 mg.

B. Measurement

Magnetization was measured by two Quantum Design vibrating sample magnetometers (VSMs). Extensive magnetic measurements by both us and the staff of Quantum Design (up to 1100 K) on a control sample of Er_2O_3 show that the absolute accuracy of the moment is better than 1.0×10^{-7} emu at low fields after correcting for a constant offset of 5.0×10^{-7} emu due to the interaction between the VSM drive head and the pick-up coils (see below). Fields between 0.03 Oe and 15 Oe are

obtained by using the ultra low-field option. The magnitude and direction of the field profile were measured by a flux-gate device. The oven option is rated for temperatures up to 1100 K, but we successfully pushed the temperature up to 1200 K in three runs. In the fourth run, the heater broke at about 1132 K. The sample chamber is in a high vacuum ($<10^{-4}$ torr) during measurements, which prevents the carbon nanotubes from burning. The VSM oscillation frequency is 40 Hz and the oscillation amplitude is 1 mm. When the sample is inserted into the sample chamber, it first experiences a positive (upward) field of about 200 Oe and then the same negative (downward) field due to the presence of the linear motor used to vibrate the sample. The magnetic hysteresis loop was measured for the sample holder alone (including the heater stick, Zircar cement, and copper foil) at 300 K. The saturation moment is 5.4×10^{-6} emu and the linear moment per Oe is -4.3×10^{-9} emu. Such a saturation moment corresponds to about 5.4×10^{-5} mg of magnetic impurities if we take a typical saturation magnetization of 100 emu/g. Our sample masses range from 5 mg to 41 mg, which are 10^5 - 10^6 times larger than the mass of magnetic impurities in the sample holder. Therefore, the magnetic signal from the sample holder is negligible compared with our sample signal.

III. RESULTS AND DISCUSSION

A. Experimental results for a control sample of Er_2O_3 : Determinations of measurement accuracies

Because of the high temperature, low field and high sensitivity requirements of this work, we worked closely with the staff of Quantum Design to define the measurement accuracies in moment and temperature. Prior to this work, Quantum Design's VSM was rated for temperature up to 1000 K and for moment $< 7 \times 10^{-7}$ emu. After we made extensive magnetic measurements on a control sample of Er_2O_3 up to 1100 K, we find that the temperature is accurate up to at least 1100 K and the absolute accuracy in moment can be better than 1×10^{-7} emu in low fields. We believe that the temperature reading is also reliable above 1100 K except that there is a risk in breaking the heater stick for temperatures higher than 1100 K.

Fig. 1 shows the temperature dependence of the field-cooled susceptibility for a 9.4 mg Er_2O_3 sample in a field of 10 kOe. The cooling rate for this measurement is 10 K per minute. We can fit the data by the Curie-Weiss law

$$\chi = \frac{C}{T + \theta}, \quad (1)$$

where C is the Curie constant. The solid line is the fitted curve which lies almost perfectly on the top of data points. The best fit gives $C = (6.327 \pm 0.002) \times 10^{-2}$

emu/g and $\theta = 24.2 \pm 0.2$ K. We also fit warm-up data by Eq. 1. The best fit gives $C = (6.304 \pm 0.002) \times 10^{-2}$ emu/g and $\theta = 16.7 \pm 0.2$ K. The Curie constants deduced from the cool-down and warm-up data differ only by 0.36%. The θ values differ by 7.6 K, suggesting that there is a small thermal lag of about 3.8 K for the heating/cooling rate of 10 K per minute. For the heating/cooling rate of 100 K per minute, there is a thermal lag of about 20 K. For most measurements on the nanotube samples, the heating/cooling rate is 50 K per minute and thus the thermal lag should be less than 20 K.

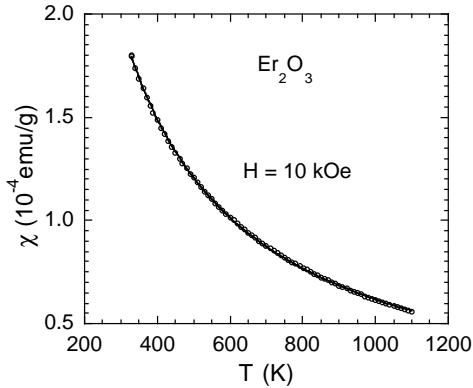


FIG. 1. The temperature dependence of the field-cooled susceptibility for a 9.4 mg Er_2O_3 sample in a field of 10 kOe. The data shown are thinned for clarity. The solid line is a fit to all the data points by the Curie-Weiss law.

The intrinsic θ value for the Er_2O_3 sample is determined to be 20.5 K by taking a simple average of the two θ values. From the Curie constants, we can easily calculate the effective magneton number of Er^{3+} to be 9.8, which is about 2% larger than the theoretical prediction (9.6). This small discrepancy may arise from the uncertainty in the sample weight.

Since the moments of the Er_2O_3 sample in 10 kOe are in the range between 0.005-0.016 emu, which are far above the instrument resolution, the data must be very accurate. Therefore, by comparing these accurate data with those data taken in the low field range, we can determine the absolute accuracy of the moment. In Fig. 2, we show the temperature dependencies of the offset moments in the fields of 0.06 Oe and 4.21 Oe, respectively. The data shown are thinned for clarity. The offset moments are obtained by subtracting the above determined Curie-Weiss term from the raw data. In the field of 0.06 Oe, the Curie-Weiss term is very small (e.g., 1.17×10^{-7} emu at 300 K), so the offset moments dominate in the whole temperature region. Since the data are taken with 3 second per point averaging, there is significant data scattering. We can average the data by using an 8th order polynomial fit to all the data points (dotted line). The averaged curve shows no sizable temperature dependence. Then

we simply fit the data by a constant line (solid line). The best fits to the 0.06 Oe and 4.21 Oe data give $m_{\text{offset}} = (4.54 \pm 0.07) \times 10^{-7}$ emu and $(5.20 \pm 0.05) \times 10^{-7}$ emu, respectively.

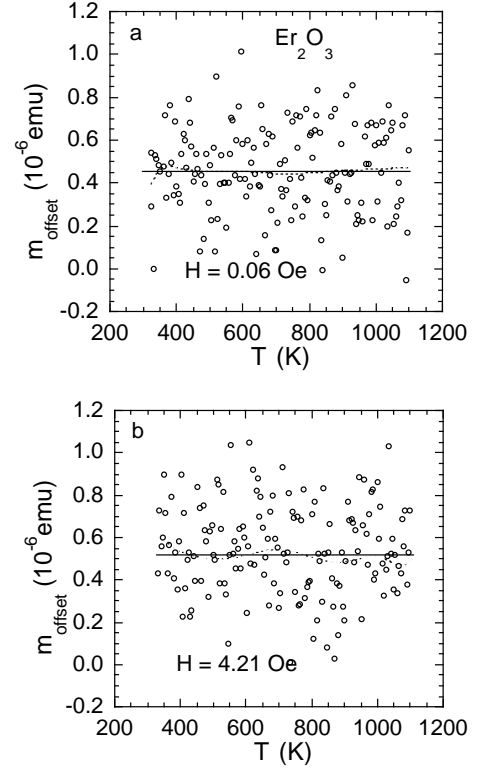


FIG. 2. The temperature dependencies of the offset moments in the fields of a) 0.06 Oe and b) 4.21 Oe, respectively. The data shown are thinned for clarity. The offset moments are obtained by subtracting the above determined Curie-Weiss term from the raw data.

Fig. 3 shows the field dependence of the offset moment. The offset moments determined from both cool-down and warm-up data are included in the figure for comparison. It is clear that the offset moments are centered around 5.0×10^{-7} emu in this low-field range (0.06-4.21 Oe). The maximum deviation from 5.0×10^{-7} emu is 0.46×10^{-7} emu. This offset moment has negligible field and temperature dependencies relative to our signals of interest and is caused by the interaction between the VSM drive head and the pick-up coils. Therefore, if we correct low-field moments by the constant offset moment, the absolute accuracy of the corrected moments should be better than 0.6×10^{-7} emu. In other words, if we use a proper averaging for data points and correct for the constant offset of 5.0×10^{-7} emu, the absolute accuracy of the corrected moment can be better than 1×10^{-7} emu. We thus correct all the following data by the constant offset of 5.0×10^{-7} emu. Since the following data were collected with 10 second per point averaging, the data scattering is significantly reduced.

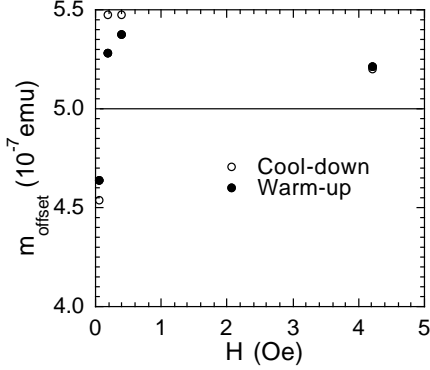


FIG. 3. The field dependence of the offset moment determined by fitting both cool-down and warm-up data. The offset moments are centered around 5.0×10^{-7} emu. The maximum deviation from 5.0×10^{-7} emu is 0.46×10^{-7} emu. The constant offset moment is caused by the interaction between the VSM drive head and the pick-up coils.

B. Superconductivity in AD prepared samples

The concentration of magnetic contaminants in AD prepared samples should be very small since the samples were prepared by arc discharge process without metal catalysts. Nevertheless, a very small amount of magnetic impurities could have a dominant contribution to magnetic properties of a sample if the intrinsic magnetic susceptibility of the sample is small. Therefore, it is important to accurately determine the concentration of magnetic contaminants in the AD prepared samples before we can draw any meaningful conclusions from the magnetic data.

Fig. 4a shows the field-cooled susceptibility in 100 Oe for a 14.6 mg AD prepared sample. The sample was heated up to 1000 K in 100 Oe and cooled down from 1000 K in the same field. At about 875 K, the susceptibility increases sharply, indicating ferrimagnetic/ferromagnetic ordering with a Curie temperature (T_C) of about 875 K. From the Curie temperature, we can conclude that this AD prepared sample is contaminated with Fe_3O_4 magnetic impurities. At 1000 K, we also see that the susceptibility increases rapidly with time. This could be caused by a thermal lag and/or by the reduction of Fe_3O_4 to Fe which has a Curie temperature of 1043 K. The ferrimagnetic component can be estimated by subtracting the extrapolated line in the figure from the total susceptibility. In Fig. 4b we plot the estimated ferrimagnetic component of the susceptibility. The temperature dependence of the susceptibility appears to be in good agreement with that for a typical ferromagnet. At 600 K, the ferrimagnetic susceptibility of the Fe_3O_4 impurities is about 3.0×10^{-6} emu per gram of MWNT sample.

We can fit the ferrimagnetic component of the susceptibility near T_C by an equation:

$$\chi_{FM}(T) = \chi_{FM}(0)[1 - (T/T_C)^p]. \quad (2)$$

The best fit gives $T_C = 876.7$ K, $p = 23.75$, and $\chi_{FM}(0) = 2.5 \times 10^{-6}$ emu/g. It is clear that the fitted curve is significantly underestimated at temperatures well below T_C .

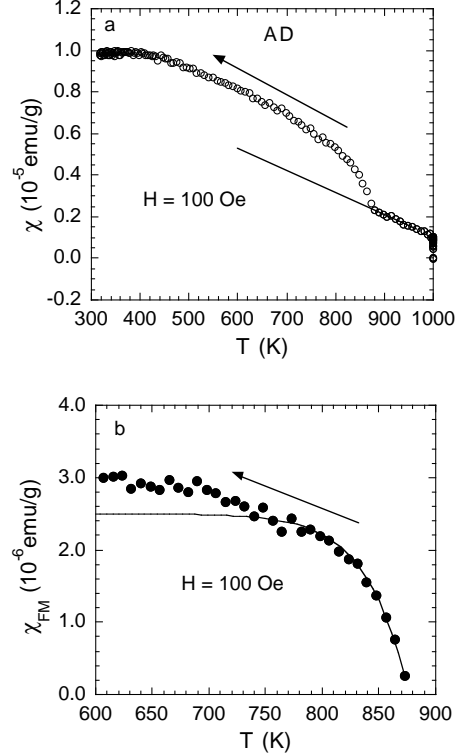


FIG. 4. a) The field-cooled susceptibility in 100 Oe for a 14.6 mg AD prepared sample. b) The estimated ferrimagnetic component of the susceptibility due to magnetic impurities. The data are fitted by Eq. 2 with $T_C = 876.7$ K, $p = 23.75$, and $\chi_{FM}(0) = 2.5 \times 10^{-6}$ emu/g.

We remind ourselves that for materials lightly contaminated with magnetic impurities having large permeabilities, the low field susceptibility is independent of the permeability and depends only on the shape (demagnetization factor) and concentration of the contaminant. The shape effect is averaged out through a random orientation so that the average demagnetization factor N should be about $1/3$ and the low-field susceptibility should be $1/(4N\pi) = 0.24$ emu/cm³. Since the specific weight of Fe_3O_4 is 5.3 g/cm³, we easily calculate the low-field susceptibility of pure Fe_3O_4 particles to be 0.045 emu/g. The specific weight of Fe is 7.9 g/cm³, so the low-field susceptibility of pure Fe particles is 0.030 emu/g. This implies that the concentration of the Fe_3O_4 impurities in the AD prepared sample is about $3 \times 10^{-6}/0.045 = 67$ ppm. If the step-like increase of the susceptibility at 1000 K (1.2×10^{-6} emu/g) could arise from the reduction of Fe_3O_4 to Fe, the concentration of the reduced Fe_3O_4 would be about 27 ppm. Then the upper limit of the total Fe_3O_4 impurity concentration is about 94 ppm. If

the Fe_3O_4 impurities are completely reduced to Fe, the upper limit of the Fe impurities is about 66 ppm.

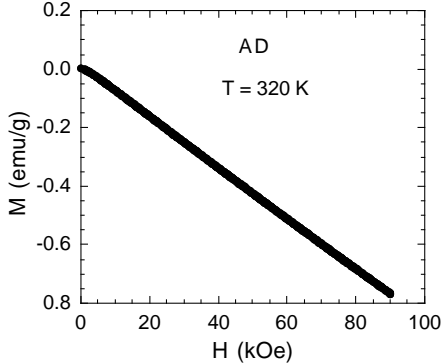


FIG. 5. The field dependence of the magnetization at 320 K for the 14.6 mg AD prepared sample. Between 20 kOe and 90 kOe, the data can be excellently fitted by a linear relation $M = M_s + \chi_{dia}H$ with $M_s = 9.27 \times 10^{-3}$ emu/g and $\chi_{dia} = -8.66 \times 10^{-6}$ emu/g.

The total concentration of ferromagnetic and/or ferrimagnetic impurities in the AD prepared sample can also be estimated from the field dependence of the magnetization at 320 K, as shown in Fig. 5. Above 20 kOe, the magnetization of any ferromagnetic impurity should be saturated and independent of the field. Between 20 kOe and 90 kOe, the data can be excellently fitted by a linear relation $M = M_s + \chi_{dia}H$ with $M_s = 9.27 \times 10^{-3}$ emu/g and $\chi_{dia} = -8.66 \times 10^{-6}$ emu/g. The field independent diamagnetic susceptibility in the high-field region could be consistent with granular superconductivity, as observed in the granular superconductor $\text{Tl}_2\text{Ba}_2\text{CuO}_{6+y}$ with $T_c = 15$ K (see Fig. 7 of Ref. [12]). If individual multi-walled carbon nanotubes are superconductors, it is natural that multi-walled nanotube mat samples are granular superconductors. Given that the saturation magnetization of a typical ferromagnet/ferrimagnet is about 100 emu/g, the deduced saturation magnetization from the fit corresponds to about 100 ppm magnetic impurities.

Fig. 6 shows the temperature dependence of the magnetization in a field of 0.03 Oe for an identical AD prepared sample, but with a mass of 41 mg. When the sample is inserted into the sample chamber with a field of 0.03 Oe, it first experiences a positive (upward) field of about 200 Oe and then the same negative (downward) field due to the presence of the linear motor used to vibrate the sample. Therefore the warm-up magnetization is the sum of the negative remanent magnetization and the non-remnant magnetization in 0.03 Oe. It is clear that the negative magnetization flattens out above 700 K and that there is a nearly temperature-independent negative magnetization between 700 K and 900 K. Above 900 K, the magnetization increases sharply, reaches a peak at about 1142 K and then drops sharply between 1142 K and 1170 K.

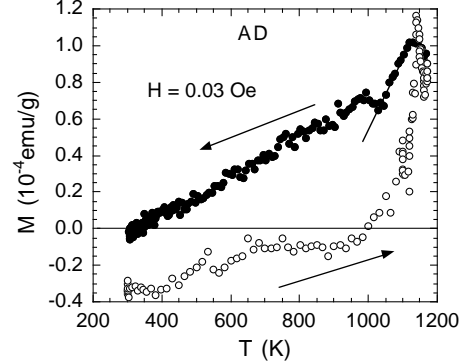


FIG. 6. a) The temperature dependence of the magnetization in a field of 0.03 Oe for a 41 mg AD prepared MWNT mat sample.

When the sample is cooled from 1170 K, the magnetization does not go back to the warm-up curve, showing a significant hysteresis. At about 1030 K, we see a dip in the cool-down magnetization, which could reveal the onset of the ferromagnetic ordering of Fe. The Curie temperature of Fe determined from these FC data is about 10 K lower than the expected value (1043 K). This is caused by a thermal lag of about 10 K for the cooling rate of 50 K per minute. At 875 K, we do not see an anomaly associated with ferrimagnetic ordering of the Fe_3O_4 impurities. It is very likely that the Fe_3O_4 impurities have almost completely been reduced into Fe after the sample was heated up to 1170 K at a high vacuum.

The ferromagnetic component (due to the Fe impurities) in the cool-down data can be estimated by subtracting the extrapolated line in Fig. 6 from the total magnetization. In Fig. 7a we plot the estimated ferromagnetic component of the susceptibility. The solid line is the fitted curve by Eq. 2. The best fit gives $T_C = 1030.6$ K, $p = 14.56$, and $\chi_{FM}(0) = 1.46 \times 10^{-3}$ emu/g. In Fig. 7b, we show the intrinsic FC susceptibility of the carbon nanotubes after subtracting the fitted curve of Fig. 7a from the total susceptibility. We see that the susceptibility drops by about 5.0×10^{-3} emu/g when the temperature is lowered from 1130 K to 305 K. This implies that the magnitude of the diamagnetic component at 305 K is at least 5.0×10^{-3} emu/g, which corresponds to about 14% of the full Meissner effect ($-1/4\pi$) given that the specific weight of multi-walled nanotubes is 2.17 g/cm³. It is interesting to note that the diamagnetic susceptibility at 305 K is about -1.55×10^{-3} emu/g, corresponding to about 4% of the full Meissner effect. This large FC susceptibility is *only* consistent with superconductivity.

This temperature dependence of the intrinsic FC susceptibility is similar to that observed in a Nb disk (see Fig. 1 of [13]). Such a temperature dependence can arise from the interplay between the diamagnetic screening currents (diamagnetic Meissner effect) and the paramagnetic circulating currents (paramagnetic Meissner effect) around the vortices [14]. The diamagnetic component of

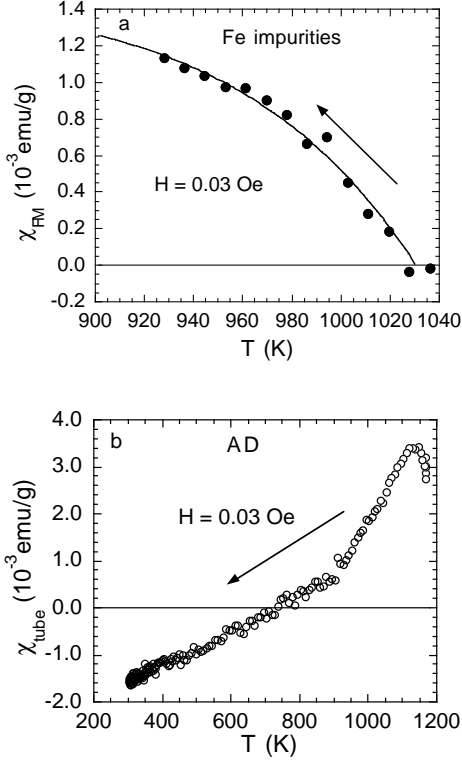


FIG. 7. a) The estimated FC ferromagnetic susceptibility due to Fe impurities in the AD prepared MWNT mat sample. b) The intrinsic FC susceptibility of the carbon nanotubes after subtracting the fitted curve of Fig. 7a from the total susceptibility. The diamagnetic susceptibility at 305 K is about -1.55×10^{-3} emu/g, corresponding to about 4% of the full Meissner effect ($-1/4\pi$).

the susceptibility should be nearly independent of the magnetic field H when H is below the lower critical field H_{c1} of a bulk sample. This is indeed the case for the Nb disk [13]. On the other hand, for a granular superconductor, the intergrain lower critical field tends to zero due to a very large intergrain penetration depth. In the low field region, the magnitude of the diamagnetic susceptibility is found to increase with decreasing field much faster than $1/H$ (see Ref. [12,15,16]) so that the diamagnetic component can be significant only in the low field range.

Moshchalkov, Qiu, and Bruyndoncx (MQB) [14] suggested that the paramagnetic Meissner effect (PME) can be caused by the persistence of the giant vortex state with the fixed orbital quantum number $L > 0$. This state is formed in any finite-size superconductor at the third surface critical field H_{c3} , which is higher than the bulk upper critical field H_{c2} for smooth and clean surfaces. According to this model [14], the PME in small diameter superconducting wires is particularly strong because of the larger surface to volume ratio. This model can naturally explain why a Pb nanowire array with an average diameter of 40 nm is paramagnetic down to 2 K while another Pb nanowire array with a diameter of 60 nm is

diamagnetic below about 3.8 K in the FC condition [17].

From the fitted curve in Fig. 7a, we find that the ferromagnetic susceptibility at low temperatures is about 1.46×10^{-3} emu/g. If there were no superconductivity in the nanotubes, this ferromagnetic susceptibility would be too large to be consistent with the above determined upper limit of the Fe impurity concentration (66 ppm). Without superconductivity in the nanotubes, the predicted upper limit of the low-field ferromagnetic susceptibility would be 0.000066×0.03 emu/g = 2.0×10^{-6} emu/g, which is a factor of about 700 smaller than the deduced 1.46×10^{-3} emu/g. In order to understand this large enhancement in the low-field ferromagnetic susceptibility of the Fe impurities, one must assume that the effective fields on the magnetic impurity sites are greatly enhanced compared with the applied field, that is, $H_{eff}/H \gg 1$. This is possible only if the host material (carbon nanotubes) exhibits superconductivity above the Curie temperature of magnetic impurities and some fraction of the impurities are flux pinning centers. It is known that the effective fields on those pinning centers are close to the lower critical field H_{c1} . If the lower critical field inside grains (bundles) is 100 Oe and 20% of the magnetic impurities are pinning centers, then the ferromagnetic susceptibility in the field of 0.03 Oe will increase by a factor of 660.

The PME is mostly seen in FC data [18]. However, the PME is also seen in zero-field-cooled (ZFC) data of granular superconductors [15,16,19]. The authors of the MQB theory [14] have assumed that the system only goes to the diamagnetic $L = 0$ state in the ZFC condition so that the PME does not exist in ZFC data. We do not think that this assumption is justified. Since all the $L \geq 0$ states are the solutions of the Ginzburg-Landau equations in mesoscopic samples [14], these states should not behave very differently. For the $L = 0$ state, it is well known that the FC and ZFC diamagnetic susceptibilities are the same for superconducting samples without open holes. By analogy, the FC and ZFC paramagnetic susceptibilities for samples without open holes should not have a substantial difference in the case of the $L > 0$ states. Because Gibbs energies for all the states are quite close near T_c (Ref. [14]), the thermal energy should be large enough to populate high- L states, leading to the paramagnetic Meissner effect. Because of the metastable nature of these states, the paramagnetic Meissner effect will strongly depend on the cooling or heating rate and on the field history, particularly if the sample never goes to the normal state. Thus the PME naturally explains the hysteresis in Fig. 6 noted earlier.

In Fig. 8a and Fig. 8b we show the ZFC susceptibility for the AD prepared sample in 15 Oe and 200 Oe, respectively. For the 15 Oe ZFC measurement, the sample was cooled from 1170 K to 300 K in “zero” field (0.03 Oe) and then the 15 Oe field was set at 300 K. For the 200 Oe ZFC measurement, the sample was cooled from 1200 K to 310 K in “zero” field (0.03 Oe), and then the 200 Oe

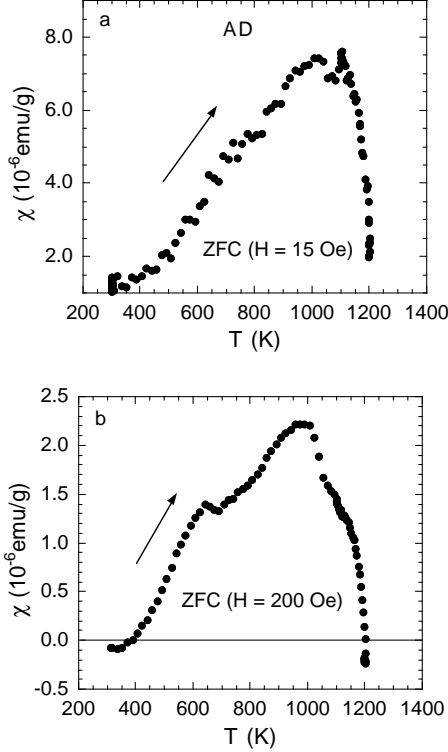


FIG. 8. The temperature dependencies of the ZFC susceptibility for the AD prepared MWNT mat sample in magnetic fields of a) 15 Oe and b) 200 Oe. The shoulder and dip features are typical of granular superconductors [15,16]. The onset of the paramagnetic Meissner effect is at about 1200 K, indicating an intragrain superconducting transition temperature of about 1200 K.

field was set at 310 K. As we learn from the data [16] of $\text{Ru}_{1-x}\text{Sr}_2\text{GdCu}_{2+x}\text{O}_{8-y}$, the onset temperature T_{cJ} of intergrain Josephson coupling approximately corresponds to either a dip-like or a shoulder-like feature. For the 15 Oe data, there is a shoulder feature near 700 K, corresponding to the onset of intergrain Josephson coupling. A sharp peak is seen at 1105 K. Between 1105 and 1200 K, the susceptibility drops sharply with temperature, indicating the onset of the PME at about 1200 K. This implies that the superconducting transition temperature is slightly higher than 1200 K because the onset of the PME is slightly lower than the intragrain superconducting transition temperature (T_c) [13,14,18,19]. For the 200 Oe data, there is a dip-like feature at about 690 K, corresponding to the onset of intergrain Josephson coupling [16]. Between 1000 and 1200 K, the susceptibility drops sharply with temperature and even becomes negative at 1200 K.

In Fig. 9, we show the ZFC susceptibility in four different fields. For the 500 Oe and 1000 Oe ZFC measurements, the sample was cooled from 1200 K to 310 K in “zero” field (about 2 Oe), and the fields were set at about 320 K. For the 15 Oe and 200 Oe ZFC measurements, the “zero” field is 0.03 Oe. A dip-like feature defines T_{cJ} for

the 200 Oe data while shoulder-like features define T_{cJ} for the 15 Oe, 500 Oe and 1000 Oe data.

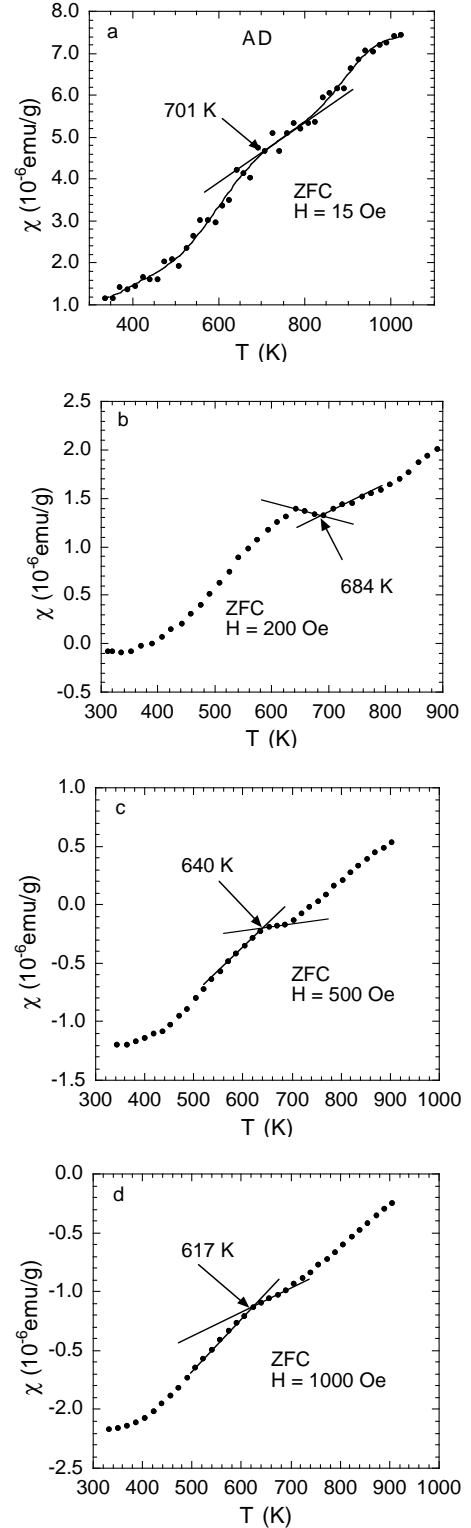


FIG. 9. The expanded views of the ZFC susceptibility for the AD prepared MWNT mat sample in the magnetic fields of a) 15 Oe, b) 200 Oe, c) 500 Oe, and d) 1000 Oe.

In Fig. 10a, we plot H versus T_{cJ} for the AD prepared MWNT mat sample. One can see that T_{cJ} depends very strongly on the magnetic field in this low field region. Such a field dependence of T_{cJ} is a hallmark of intergrain Josephson coupling [15,20]. In Fig. 10b, we show H versus T_{cJ} for the granular superconductor $\text{Ru}_{0.6}\text{Sr}_2\text{GdCu}_{2.4}\text{O}_{8-y}$. T_{cJ} is defined as the onset of the paramagnetism in the FC magnetization data in Fig. 3 of Ref. [16] and as the midpoint of the resistive transition in Fig. 6 of Ref. [16]. By comparing Fig. 10a with Fig. 10b, we can see that the field dependence of T_{cJ} has a similar form for both systems, suggesting the same physical origin: Intergrain Josephson coupling. The strong field dependence of T_{cJ} in the low field region also rules out a magnetic origin for the transition.

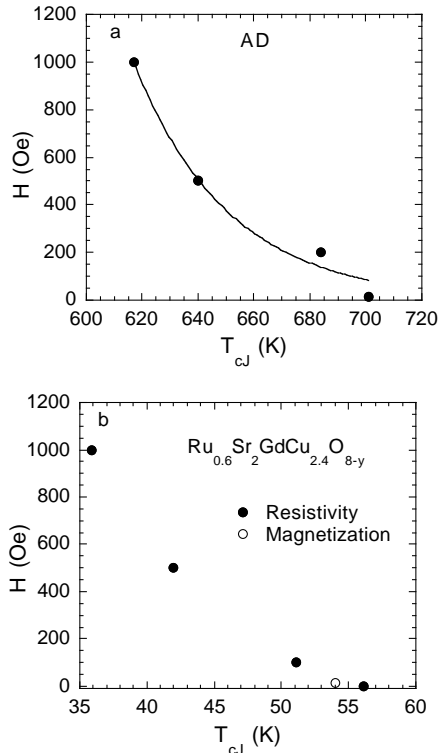


FIG. 10. The magnetic field (H) versus the onset temperature of intergrain coupling (T_{cJ}) for a) the AD prepared MWNT mat sample and b) the granular superconductor $\text{Ru}_{0.6}\text{Sr}_2\text{GdCu}_{2.4}\text{O}_{8-y}$ (Ru-1212). The solid line in Fig. 10a is a fit by an equation $H = (A/T_{cJ}) \exp(-T_{cJ}/T_o)$ with $T_o = 35.8$ K. This equation has been used to fit the H versus T_{cJ} data of a granular superconductor [15].

In Fig. 11a we plot previously published resistance data for an AD prepared MWNT mat that comes from the same lot as the AD prepared sample here. The data are the same as those reported in Ref. [8] except they are thinned here for clarity. It is interesting that the resistance decreases with increasing temperature below about 570 K while above 570 K the resistance tends to

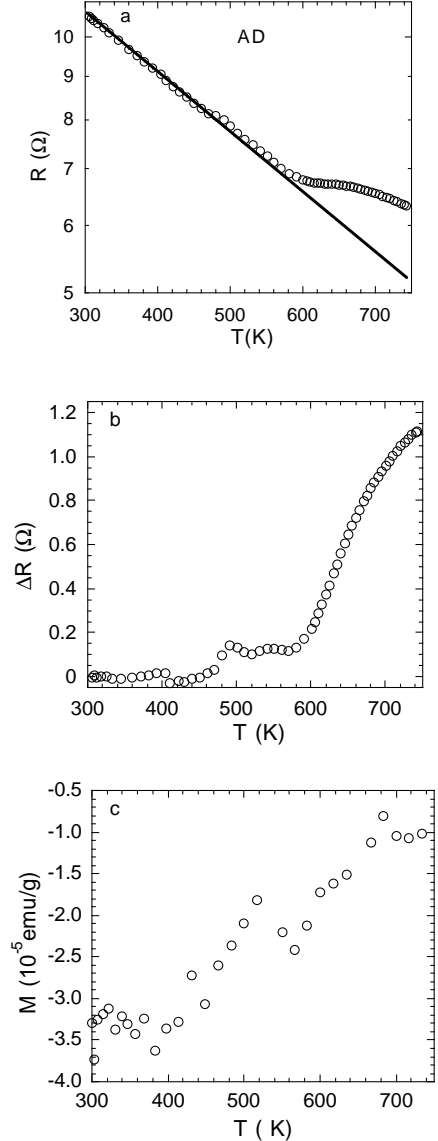


FIG. 11. a) The temperature dependence of the resistance for an AD prepared MWNT mat that comes from the same lot as those studied here. The resistance data are the same as those reported in Ref. [8] except they are thinned for clarity. A fitted curve is given by the solid line. b) The resistance data subtracted by the fitted curve. c) The expanded view of the warm-up magnetization (Fig. 6) for the AD prepared MWNT sample. The two transitions at about 500 K and 700 K in these magnetization data also emerge in the resistance data (b) for the same sample.

turn up. The resistance between 300 K and 450 K can be excellently described by $17.3 \exp(-T/618.3) \Omega$. This semiconducting-like resistance may come from the intertube barrier resistance for some extremely weak Josephson junctions in the percolative network. These Josephson junctions are too weakly coupled to lead to a zero-resistance state. Instead, the ground state is insulating in these extremely weakly coupled junctions. On the

other hand, from Fig. 9 we see that some other Josephson junctions in the mat sample are strongly coupled so that the onset temperature of intergrain Josephson coupling is around 700 K. This suggests that our mat samples consist of both weakly and strongly coupled Josephson junctions.

In order to more clearly see the resistive transition, we plot in Fig. 11b ΔR , the resistance data subtracted by the fitted curve. These ΔR data should represent the resistive behavior in some parts of the mat sample, which have a rather strong Josephson coupling. In addition to the major transition at about 700 K, consistent with the T_{cJ} value deduced from the magnetic data above, there appears to be a second transition at about 500 K. This second transition may be related to weaker Josephson coupling in some regions of the mat sample resulting in this lower T_{cJ} .

In Fig. 11c, we show an expanded view of the warm-up magnetization below 750 K for the AD prepared MWNT sample. We clearly see that there is a rapid drop in the magnetization below 700 K. In addition to the clear anomaly at about 700 K, there is also an anomaly at about 500 K in the magnetization data. It is striking that both anomalies are also seen in the resistance data (Fig. 11b). This one-to-one correspondence between the transitions in the magnetic and electrical data in the same sample provides additional evidence for hot superconductivity in AD prepared multi-walled carbon nanotubes.

C. Superconductivity in sample CVD1

Fig. 12a shows the temperature dependence of the warm-up magnetization in a field of -0.06 Oe for sample CVD1. When the sample is inserted into the sample chamber with a field of -0.06 Oe, it first experiences a positive field of about 200 Oe and then the same negative field due to the presence of the linear motor used to vibrate the sample. Therefore, the warm-up magnetization is the sum of the negative remanent magnetization and the non-remnant magnetization in -0.06 Oe. It is apparent that the negative magnetization has a kink feature at about 530 K and that the magnetization flattens out above 880 K. The small constant magnetization between 880 and 1000 K (represented by the horizontal line) in the warm-up data is the same as that in the cool-down data. Thus, the reversible constant magnetization between 880 and 1000 K is the nonremnant magnetization, which suggests a ferrimagnetic/ferromagnetic ordering at about 880 K. From the Curie temperature of 880 K, we conclude that this CVD prepared sample also contains Fe_3O_4 magnetic impurities.

Assuming this small constant nonremnant magnetization extends to the temperature region between 300 and 880 K, we obtain the remanent magnetization by

subtracting this small constant term from the total magnetization, as shown in Fig. 12b. The remanence above 530 K can be well fitted by an equation

$$M_r(T) = M_r(0)[1 - (T/T_C)^q]. \quad (3)$$

The solid line is the fitted curve with a fixed parameter $T_C = 880$ K and two fitting parameters: $q = 1.5$ and $M_r(0) = -0.0024$ emu/g. The value of $q = 1.5$ is typical for multidomain ferromagnetic particles.

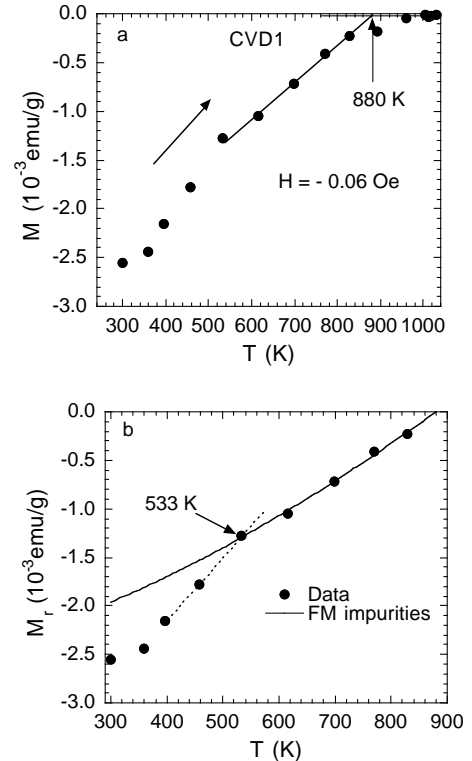


FIG. 12. a) The temperature dependence of the warm-up magnetization in a field of -0.06 Oe for sample CVD1. b) The temperature dependence of the remanent magnetization for sample CVD1. The solid line represents the ferrimagnetic remanence due to the Fe_3O_4 magnetic impurities.

From Fig. 12b, we see that an extra remanence sets in below about 530 K. This extra contribution should be associated with a second transition which could be the onset of intergrain Josephson coupling or a ferromagnetic/ferrimagnetic transition. We can make a clear distinction between these two interpretations by studying the field dependence of this transition. If this transition very strongly depends on the magnetic field, it must be related to the onset temperature of intergrain Josephson coupling.

Fig. 13a shows the temperature dependencies of the FC susceptibility for sample CVD1 with different magnetic fields. One can see that there is a ferromagnetic/ferrimagnetic phase transition with the Curie temperature T_C of about 870 K. This is consistent with the

remance data in Fig. 12b.

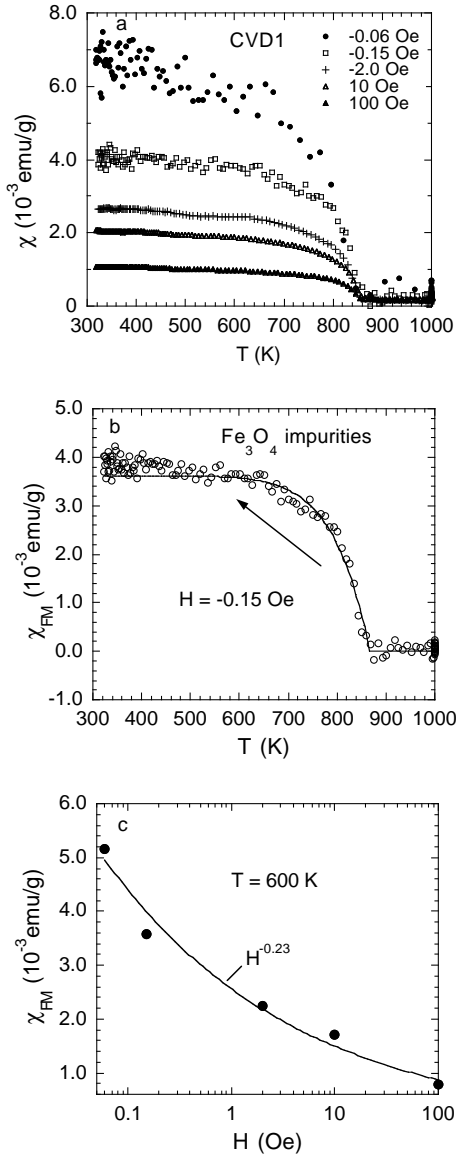


FIG. 13. a) The temperature dependence of the FC susceptibility for sample CVD1 with different magnetic fields. b) The temperature dependence of the ferrimagnetic component of the susceptibility in the field of -0.15 Oe. c) The ferrimagnetic component of the susceptibility at 600 K versus H for sample CVD1.

In Fig. 13b we plot the temperature dependence of the ferrimagnetic component of the susceptibility in the field of -0.15 Oe. The ferrimagnetic component is estimated by subtracting a small constant paramagnetic term—evident between T_C and 1000 K—from the total susceptibility. The solid line is a fit by Eq. 2 with the fitting parameters: $T_C = 867.6$ K and $p = 11.66$. This p value is very close to that for the Fe impurities in the AD sample (see Fig. 7a). In Fig. 13c, we plot the ferrimagnetic component of the susceptibility at 600 K versus H for sample CVD1. It is

clear that the ferrimagnetic susceptibility decreases with increasing H , which follows a power law: $\chi_{FM} \propto H^{-0.23}$.

This unusual field dependence is hard to explain if there were no superconductivity in the nanotubes. From the measured magnetic hysteresis loop at 300 K, we obtain the saturation magnetization of 1.4 emu/g. Since the saturation magnetization of pure Fe_3O_4 particles is 92 emu/g at room temperature, we estimate that the sample has 1.5% Fe_3O_4 magnetic impurities, which would lead to a low-field susceptibility of 0.015×0.045 emu/g = 6.75×10^{-4} emu/g. From Fig. 13c, we see that the ferrimagnetic susceptibility in 0.06 Oe is 0.0052 emu/g, which is about one order of magnitude larger than our predicted value (6.75×10^{-4} emu/g). On the other hand, the estimated ferrimagnetic susceptibility in 100 Oe is only 18% larger than the predicted value. If superconductivity exists in the nanotubes, some fraction of the magnetic impurities will be the flux pinning centers where the effective field is close to H_{c1} . Within this picture, the ferrimagnetic susceptibility will be greatly enhanced in the field region where $H_{c1}/H \gg 1$ while the enhancement vanishes for $H > H_{c1}$. Then, if 0.6% of magnetic impurities are the pinning centers, the ferrimagnetic susceptibility in the field of 0.06 Oe will increase by one order of magnitude. The percentage of magnetic impurities being the pinning centers should strongly depend on the field and thermal history. Fluxes can be effectively trapped if the sample is cooled in a field above T_C . This implies that the percentage is larger when the sample is cooled from a higher temperature. It is also known that more fluxes will be trapped at higher fields. Thus when the field increases the percentage of the impurities being pinning centers increases. However, if this percentage increasing rate is lower than the decreasing rate of H_{c1}/H , the ferrimagnetic susceptibility will decrease with increasing field. This may explain the field dependence of the ferrimagnetic susceptibility in sample CVD1 (Fig. 13c).

In Fig. 14, we show the expanded views of the FC susceptibility for sample CVD1 with different fields. In this temperature region, the susceptibility of the ferrimagnetic impurities increases weakly with decreasing temperature (a negative slope). There is an additional onset of paramagnetism, which is clearly seen in all the figures. This local onset of paramagnetism could be consistent with ferromagnetic/ferromagnetic ordering or the onset of intergrain Josephson coupling [16]. As one can clearly see from Fig. 14, the onset temperature depends very strongly on the magnetic field. Therefore this transition is *only* consistent with the onset of intergrain Josephson coupling.

We define the crossing temperature of the two straight lines in Fig. 14 to be T_{cJ} . In Fig. 15, we show H versus T_{cJ} for sample CVD1. It is striking that T_{cJ} depends very strongly on the field in the low field region, but becomes weakly field dependent in higher fields. This behavior is

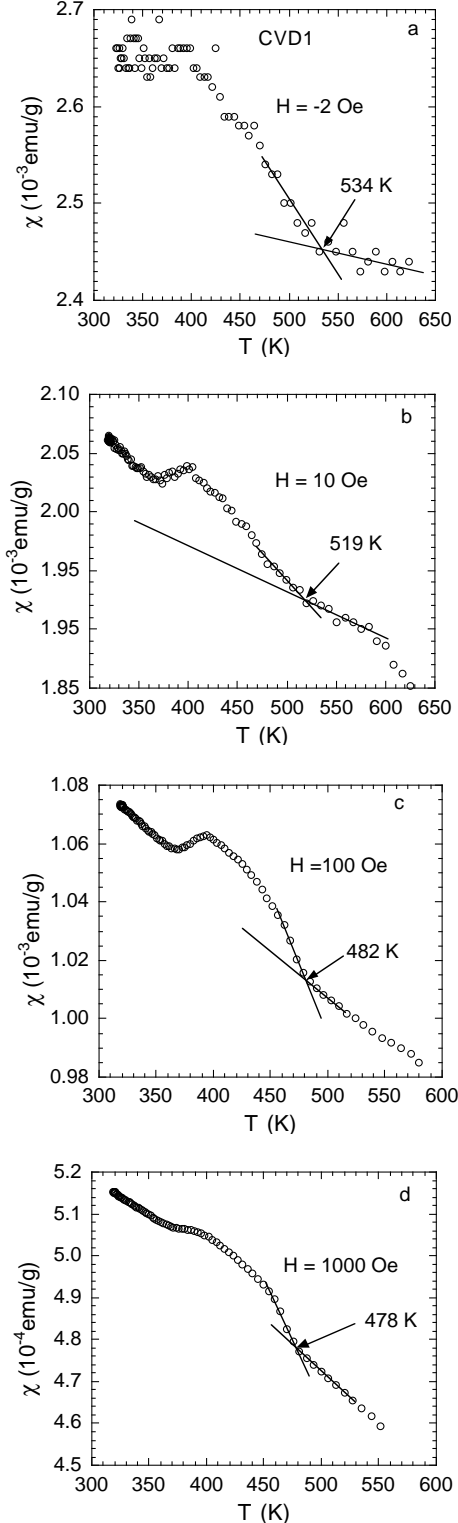


FIG. 14. The expanded views of the FC susceptibility for sample CVD1 in the magnetic fields of a) 2 Oe, b) 10 Oe, c) 100 Oe, and d) 1000 Oe.

very similar to that observed in granular superconductors [15,16,20]. The strong field dependence of T_{cJ} rules out a magnetic origin of this transition. Further, there is a

drop in the susceptibility about 100 K below T_{cJ} . This feature is also consistent with that observed in granular superconductors [15,16].

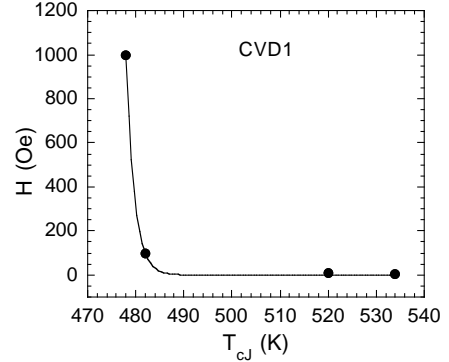


FIG. 15. H versus T_{cJ} for sample CVD1. The solid line is a fit by an equation $H = (A/T_{cJ}) \exp(-T_{cJ}/T_0)$ with $T_0 = 1.75$ K.

Another important signature of granular superconductivity is the disappearance of the superconducting remanence above T_{cJ} (see Ref. [15,16]). As shown in Fig. 12b, the ferrimagnetic remanence dominates above 533 K in this CVD sample, that is, the superconducting remanence is substantial only below 533 K and nearly disappears above 533 K. Thus the remanence data provide evidence for $T_{cJ} = 533$ K in 0.06 Oe. This is in excellent agreement with that determined from the susceptibility data (see Fig. 15).

D. Superconductivity in sample CVD2

Fig. 16a shows a zoomed view of the warm-up magnetization in a field of 0.08 Oe for sample CVD2. The virgin sample is inserted into the sample chamber with a field of 0.08 Oe after it first experiences a positive field of about 200 Oe and then the same negative field. So the warm-up magnetization is the sum of the negative remanent magnetization and the non-remnant magnetization in 0.08 Oe. It is remarkable that the negative magnetization has a kink feature at about 700 K and that the magnetization flattens out above 875 K. The constant magnetization between 875 and 1000 K (represented by the horizontal line) is the nonremnant magnetization in this temperature region. These data imply a ferrimagnetic/ferromagnetic ordering at about 875 K. From the Curie temperature, we conclude that this CVD prepared sample also contains Fe_3O_4 magnetic impurities. Since the total impurity concentration in this sample is about 0.3%, the concentration of Fe_3O_4 magnetic impurities should be less than 0.3%.

Assuming this small constant nonremnant magnetization extends to the temperature region between 300

and 875 K, we obtain the remanent magnetization by subtracting this small constant term from the total magnetization, as shown in Fig. 16b. The remanence above 700 K is fitted by Eq. 3. The solid line is the fitted curve with two fixed parameters $T_C = 875$ K and $q = 1.5$, and one fitting parameter $M_r(0) = 3.07 \times 10^{-4}$ emu/g. The fitted solid line represents the ferrimagnetic remanence contributed from the Fe_3O_4 impurities. The large extra contribution below 700 K is associated with a second transition which should be the onset of intergrain Josephson coupling.

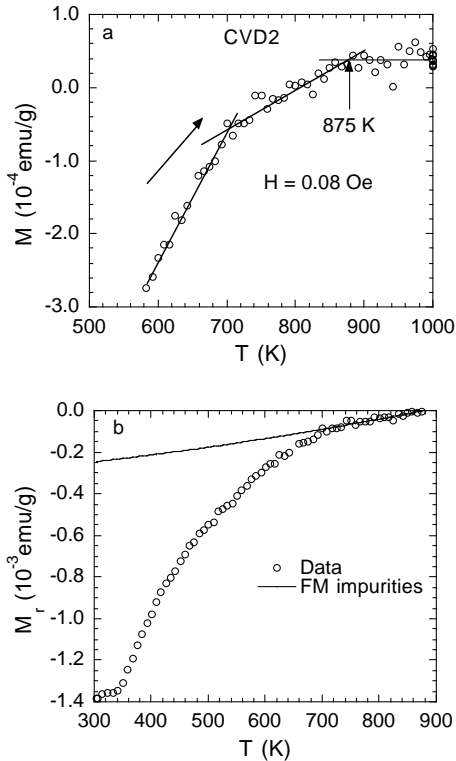


FIG. 16. a) The temperature dependence of the warm-up magnetization in a field of 0.08 Oe for sample CVD2. b) The temperature dependence of the remanent magnetization for sample CVD2. The solid line represents the ferrimagnetic remanence due to the Fe_3O_4 magnetic impurities.

Fig. 17a shows the temperature dependence of the field-cooled susceptibility in a field of 0.08 Oe for sample CVD2. The data appear to indicate two ferromagnetic/ferrimagnetic transitions at about 864 K and 1028 K, respectively, although the large data scattering may mimic a single transition at about 1000 K. The former transition should be related to the ferrimagnetic ordering of the Fe_3O_4 impurities while the latter transition is associated with the ferromagnetic ordering of the Fe impurities. The Fe impurities may be reduced from some Fe_3O_4 impurities when the sample is heated to 1100 K in a high vacuum.

Fig. 17b shows the temperature dependence of the fer-

rimagnetic component of the susceptibility in the field of 0.08 Oe. This component is obtained by subtracting a constant paramagnetic term—evident between 1030 K and 1100 K—from the total susceptibility. The solid line is the fitted curve by Eq. 2 with a fixed parameter $T_C = 1028$ K and two fitting parameters: $\chi_{FM}(0) = 0.00148$ emu/g and $p = 2.67$. The small p value for sample CVD2 is consistent with the fact that this sample has two magnetic transitions which, due to the large data scattering, could resemble a single broad transition.

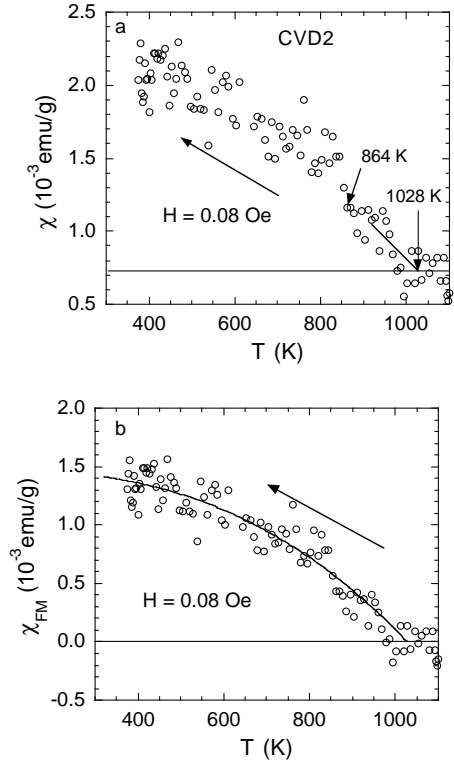


FIG. 17. a) The temperature dependence of the field-cooled susceptibility in a field of 0.08 Oe for sample CVD2. b) The temperature dependence of the ferrimagnetic component of the susceptibility in the field of 0.08 Oe. The solid line is the fitted curve by Eq. 2 with a fixed parameter $T_C = 1028$ K and two fitting parameters: $\chi_{FM}(0) = 0.00148$ emu/g and $p = 2.67$.

Comparing Fig. 17b with Fig. 13c, we see that the ferrimagnetic susceptibility at 600 K for sample CVD2 is about a factor of 5 smaller than that for sample CVD1. This is consistent with the fact that the concentration of magnetic impurities in sample CVD1 is larger than that for sample CVD2 by a factor of about 5. On the other hand, comparing Fig. 16b with Fig. 12b, we find that the ferrimagnetic remanence for sample CVD1 (from -200 Oe to -0.06 Oe) is larger than that for sample CVD2 (from -200 Oe to 0.08 Oe) by a factor of about 8. This discrepancy can be resolved if we consider the fact that the ending fields in these two cases are different. From

the lower part of the magnetic hysteresis loop of Fe_3O_4 , one can see that the magnitude of the low-field M_r decreases linearly with the increase of the ending field. The slope of the linear decrease line is approximately equal to the low-field susceptibility $\chi_{FM}(0)$. This implies that when the ending field decreases from 0.08 Oe to -0.06 Oe, the magnitude of M_r will increase by $\Delta H\chi_{FM}(0) = 0.14\chi_{FM}(0)$. Using $\chi_{FM}(0) = 0.00148$ emu/g, we find that the magnitude of M_r for sample CVD2 is $(0.000307 + 0.14 \times 0.00148)$ emu/g $= 5.1 \times 10^{-4}$ emu/g if the ending field is -0.06 Oe. Therefore, for the same ending field of -0.06 Oe, the ferrimagnetic remanence for sample CVD2 is smaller than that for sample CVD1 by a factor of about 5.

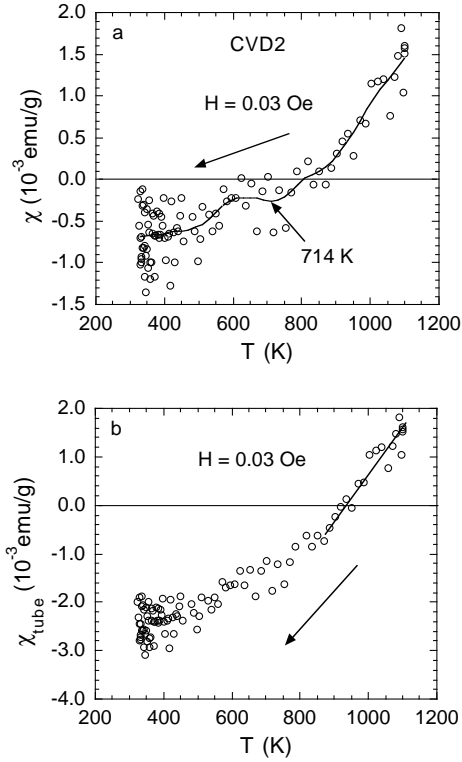


FIG. 18. a) The temperature dependence of the susceptibility in a field of 0.03 Oe for sample CVD2. The solid line is an averaged curve. The susceptibility at 330 K has a large negative value (about -6.9×10^{-4} emu/g), corresponding to about 1.9% of the full Meissner effect. b) The temperature dependence of the intrinsic susceptibility of the nanotubes. The data are obtained by subtracting the ferrimagnetic/ferromagnetic contribution from the total susceptibility. The intrinsic diamagnetic susceptibility of the nanotubes is about -2.5×10^{-3} emu/g at 330 K, corresponding to about 7% of the full Meissner effect.

Fig. 18a shows the field cooled susceptibility in a field of 0.03 Oe for sample CVD2. The sample was taken out of the VSM after the field-cooled measurement in 0.08 Oe was done. The sample was then reinserted into the sample chamber with a field of 0.03 Oe, heated up to 1100

K and cooled down in the same field. It is interesting that the susceptibility drops by about 2.2×10^{-3} emu/g when the temperature is lowered from 1100 K to 330 K. This implies that the magnitude of the diamagnetic component at 330 K is at least 2.2×10^{-3} emu/g, corresponding to about 6% of the full Meissner effect. More remarkably, the susceptibility at 330 K has a large negative value (about -6.9×10^{-4} emu/g), corresponding to about 1.9% of the full Meissner effect. From the averaged curve of Fig. 18a, we see a dip-like feature at about 700 K which corresponds to the onset of intergrain Josephson coupling. Coinciding with this temperature, we have clearly shown a large superconducting remanence up to 700 K for sample CVD2 (see Fig. 16b).

We can estimate the ferrimagnetic/ferromagnetic contribution in the field of 0.03 Oe for sample CVD2 using the field dependence of the ferrimagnetic susceptibility seen in sample CVD1 (see Fig. 13c) and the temperature dependence of the ferrimagnetic/ferromagnetic susceptibility in 0.08 Oe for sample CVD2. From Fig. 13c, we have found that $\chi_{FM} \propto H^{-0.23}$. This implies that χ_{FM} in 0.03 Oe is larger than that in 0.08 Oe by a factor of 1.25. Therefore, in the field of 0.03 Oe, $\chi_{FM}(T) = 0.00185[1 - (T/1028)^{2.67}]$ emu/g. Then the intrinsic susceptibility of the carbon nanotubes is obtained by subtracting the ferrimagnetic/ferromagnetic contribution from the total susceptibility.

Fig. 18b shows the temperature dependence of the intrinsic susceptibility of the nanotubes in sample CVD2. We can clearly see that the temperature dependence of the intrinsic susceptibility for this CVD prepared sample is similar to that for the AD prepared sample (see Fig. 7b). The intrinsic susceptibility for this CVD prepared sample decreases by 4.2×10^{-3} emu/g when the temperature is lowered from 1100 K to 330 K, corresponding to about 12% of the full Meissner effect. It is remarkable that the magnitude of the intrinsic susceptibility drop for this CVD sample is almost the same as that (4.5×10^{-3} emu/g) for the AD prepared sample. This consistency suggests that the observed large susceptibility drops in these two samples having very different masses and magnetic impurity concentrations are intrinsic to the nanotubes. Moreover, the intrinsic diamagnetic susceptibility of the nanotubes is -2.5×10^{-3} emu/g at 330 K, corresponding to about 7% of the full Meissner effect. Such a large FC diamagnetic susceptibility is *only* consistent with superconductivity.

Next we argue that the large paramagnetic susceptibility at 1100 K (1.6×10^{-3} emu/g) observed in this CVD sample cannot arise from magnetic contaminants. Since the warm-up susceptibility in 0.03 Oe coincides with the cool-down susceptibility in the temperature region between 1000 and 1100 K, there should be negligible magnetic impurities having Curie temperatures higher than 1000 K and cocervities larger than 0.03 Oe. It is highly unlikely that the sample contains magnetic impurities with Curie temperatures higher than 1100 K and with

cocervities smaller than 0.03 Oe. Furthermore, the susceptibility at 1100 K is inversely proportional to the field in the field region between 0.03-0.08 Oe (see Fig. 17a and Fig. 18), which is difficult to explain in terms of magnetic contaminations. Nevertheless, our conclusion about the existence of hot superconductivity in the nanotubes is independent of how one interprets the large paramagnetic susceptibility.

IV. CONCLUDING REMARKS

We report conclusive evidence for granular room-temperature superconductivity in multiwalled carbon nanotube mat samples with an intragrain transition temperature slightly higher than 1200 K and intergrain transition temperatures of 533-700 K. We show numerous signatures of room-temperature superconductivity: 1. a direct diamagnetic Meissner fraction of 1.9% at room temperature (this exceeds the orbital diamagnetic component by at least two orders of magnitude) 2. an inferred diamagnetic fraction of 14% at room temperature 3. coincidence of the resistive and magnetic transitions 4. existence of superconducting persistent currents (superconducting remanence) up to 700 K 5. great field sensitivity of the intergrain transition temperature and 6. very large enhancement in the low field ferrimagnetic/ferromagnetic susceptibility of magnetic impurities up to 1030 K—consistent with superconductivity above 1030 K in the nanotubes.

Another important superconductivity signature is the zero resistance state. We have clearly shown the existence of the superconducting remanence up to 700 K, implying that a zero resistance state has been achieved below 700 K in some parts of the mat samples, where both the on-tube and intergrain-Josephson-junction resistances approach zero. Further, a negligible or zero on-tube resistance has been seen in many unprocessed individual MWNTs at room temperature [21–23]. This very small on-tube resistivity has been interpreted as “ballistic transport”. Using a realistic electron-phonon coupling strength in carbon nanotubes, Zhao [10] has shown that, for a non-superconducting SWNT with a diameter of 15 nm, the on-tube resistance per unit length at room temperature is at least $367 \Omega/\mu\text{m}$, which is larger than the measured values [23] by at least one order of magnitude. The finite but very small on-tube resistance observed in individual MWNTs is a natural consequence of quantum phase slips in quasi-one-dimensional superconductors. Bundling individual MWNTs greatly suppresses quantum phase slips, leading to a nearly zero-resistance state in some parts of the mat samples.

Finally, this work is also supported by a huge chorus of facts. The single-particle gap and transition temperature—determined independently from Raman data of a SWNT mat sample—yield a ratio of 1.83 (Ref. [9]), which is close to the BCS prediction (1.76)

for weak coupling. The tunneling spectra also evidence unique superconducting signatures: The single-particle tunneling gap is found to be at least 125 meV in an individual MWNT with a diameter of 30 nm (Ref. [10]). These facts along with the present magnetic data provide compelling evidence for room-temperature superconductivity in carbon nanotubes.

Acknowledgment: We thank Quantum Design (J. O’Brien, N. R. Dilley, J. J. Cherry, R. Fox and Dan Polancic) for hospitality, use of the VSMS and technical assistance.

Correspondence should be addressed to gzhao2@calstatela.edu.

-
- [1] A. S. Alexandrov and N. F. Mott, *Polarons and Bipolarons* (World Scientific, Singapore, 1995).
 - [2] V.L. Ginzburg, in: V.L. Ginzburg, D. A. Kirzhnits Eds., *High-Temperature Superconductivity*, Consultants Bureau, New York, 1982.
 - [3] W. A. Little, Phys. Rev. **164**, A1416 (1964).
 - [4] Y. C. Lee and B. S. Mendoza, Phys. Rev. B **39**, 4776 (1989).
 - [5] S. M. Cui and C. H. Tsai, Phys. Rev. B **44**, 12500 (1991).
 - [6] R. Saito, M. Fujita, G. Dresselhaus, and M. S. Dresselhaus, Appl. Phys. Lett. **60**, 2204 (1992).
 - [7] H. Ajiki and T. Ando, J. Phys. Soc. Jpn. **62**, 1255 (1992).
 - [8] G. M. Zhao and Y. S. Wang, cond-mat/0111268.
 - [9] G. M. Zhao, *Molecular Nanowires and Other Quantum Objects*, edited by A. S. Alexandrov, J. Demsar and I. K. Yanson (Nato Science Series, Kluwer Academic Publishers, Netherlands, 2004) page 95-106.
 - [10] G. M. Zhao, *Carbon nanotubes: New Research*, edited by Frank Columbus (Nova Publisher, New York) in press.
 - [11] Y. Kopelevich, R. R. da Silva, J. H. S. Torres, S. Moehlecke, and M. B. Maple, preprint.
 - [12] C. Bergemann, A. W. Tyler, A. P. Mackenzie, J. R. Cooper, S. R. Julian, and D. E. Farrell, Phys. Rev. B **57**, 14387 (1998).
 - [13] L. Pust, L. E. Wenger, and M. R. Koblischka, cond-mat/9807109.
 - [14] V. V. Moshchalkov, X. G. Qiu, and V. Bruyndoncx, Phys. Rev. B **55**, 11793 (1997).
 - [15] H. H. Wen, W. L. Yang, Z. X. Zhao, and Y. M. Ni, Phys. Rev. Lett. **82**, 410 (1999).
 - [16] P. W. Klamut, B. Dabrowski, S. Kolesnik, M. Maxwell, and J. Mais, Phys. Rev. B **63**, 224512 (2001).
 - [17] Shijun Yuan, Liyuan Ren, and Fashen Li, Phys. Rev. B **69**, 092509 (2004).
 - [18] W. Braunisch, N. Knauf, G. Bauer, A. Kock, A. Becker, B. Freitag, A. Grutz, V. Kataev, S. Neuhausen, B. Roden, D. Khomskii, D. Wohlleben, J. Bock, and E. Preisler, Phys. Rev. B **48**, 4030 (1993).

- [19] J. Horvat, X. L. Wang, S. Soltanian and S. X. Dou, cond-mat/0201006.
- [20] R. F. Jardim, M. C. de Andrade, E. A. Early, M. M. Maple, and D. Stroud, *Physica C* **232**, 145 (1994).
- [21] S. Frank, P. Poncharal, Z. L. Wang, Walt A. de Heer, *Science* **280**, 1744 (1998).
- [22] P. J. de Pablo, E. Graugnard, B. Walsh, R. P. Andres, S. Datta, and R. Reifenberger, *Appl. Phys. Lett.* **74**, 323 (1999).
- [23] P. Poncharal, C. Berger, Y. Yi, Z. L. Wang, W. A. de Heer, *J. Phys. Chem. B* **106**, 12104 (2002).